Intermodulated fluorescence spectroscopy of BO_2 using a stabilized dye laser[a)]

R. S. Lowe,[b)] H. Gerhardt,[c)] W. Dillenschneider, R. F. Curl, Jr., and F. K. Tittel

Departments of Chemistry and Electrical Engineering, Rice University, Houston, Texas 77001
(Received 11 July 1978)

The hyperfine structure of 37 R-branch transitions involving several vibronic bands in the ground ($\tilde{X}\,^2\Pi_g$) and excited ($\tilde{A}\,^2\Pi_u$) electronic states of $^{11}BO_2$ has been observed by the technique of saturation spectroscopy with intermodulated fluorescence detection. Stabilization of the cw dye laser together with the elimination of spectral power broadening has permitted the achievement of linewidths of better than 10 MHz for a single hyperfine component. A set of plausible hyperfine constants for both electronic states determined from the observed splittings is also reported.

INTRODUCTION

A number of spectroscopic studies of the BO_2 radical have been undertaken in the past ten years using lasers as the excitation source. Russell, *et al.*,[1] analyzed the laser excited fluorescence (LEF) from several vibronic states to obtain rotational and vibrational constants for a number of levels in the $^2\Pi_g$ ground state. Muirhead, *et al.*,[2] detected hyperfine structure in one transition of BO_2 using the technique of saturation spectroscopy with intermodulated fluorescence (IMF) detection. In both of these studies, the workers were restricted to a rather narrow range of the visible spectrum by the limited tunability of an argon ion laser. Recently, the availability of broadband tunable dye laser sources has permitted several groups[3–5] to improve and extend the earlier LEF results. In light of developments in the area of frequency stabilization of dye lasers,[6,7] we undertook to extend the earlier IMF study[2] employing a high resolution cw dye laser spectrometer capable of a linewidth of better than 500 kHz. With these improvements, it was felt that sufficient data could be acquired to permit an analysis of the hyperfine coupling constants of the ground and first excited states of $^{11}BO_2$.

EXPERIMENTAL

The experiment was conducted in the Rhodamine 110 dye region (540–580 nm) where the bandheads of both the $^2\Pi_u(0,0,0) \leftarrow {}^2\Pi_g(0,0,0)$ band and the $^2\Sigma_g^+(0,1,0) \leftarrow {}^2\Sigma_u^+(0,1,0)$ band of BO_2 are located.[8] The fluorescence was excited using a Spectra Physics 580A dye laser system with 25 mW single mode output power when pumping the dye with 3 W from a Spectra Physics 170 Ar^+ laser (514.5 nm).

The long term stability of the free-running dye laser was measured at between 40 and 50 MHz. In order to improve the resolution of the saturation spectra, this linewidth was reduced using a frequency stabilization scheme similar to that discussed in Ref. 7. Briefly, a sample of the dye laser output was compared with the resonant frequency of an invar-stabilized optical reference cavity. The high frequency component (up to 50 KHz) of the resulting error signal was amplified and applied to a fast PZT mounted on a lightweight dye laser end mirror. The low frequency component (<1 KHz) was amplified by a high gain, high voltage amplifier and fed through the scan electronics of the 580A laser to the PZT on the laser's output reflector. The scanning 581A air-spaced etalon was locked to the laser cavity by modulating the etalon PZT at 1 KHz to produce an amplitude modulation of the laser which was detected, amplified at 1 KHz and phase detected with the resulting output fed back to the etalon PZT.

The BO_2 radicals were generated in a fast flow system by mixing the products of a microwave discharge of O_2 with BCl_3. The total pressure in the quartz fluorescence cell was approximately 0.1 torr and optimum fluorescence was achieved when the gas composition was adjusted to give a pale green chemiluminescence. Discrimination against scattered light was achieved by careful focussing of the fluorescence onto a 1 mm slit in front of a C31000F photomultiplier tube after passing the light through the appropriate narrow bandpass interference filter.

Assignment of the LEF was made by setting the laser to the desired absorption wavelength as observed by Johns[8] using a monochromator and surveying the adjacent region until a match with the observed optical line pattern was obtained. The density of the BO_2 spectrum required that such searches focus on locating the bandhead of a particular transition. With this as a reference point, the spacings between adjacent fluorescences were measured with the known free spectral ranges of the laser cavity and the air-spaced etalon. In this fashion, unambiguous assignment of most lines could be made.

The experimental arrangements for observing and measuring the saturation signals were similar to those developed by Sorem and Schawlow[9] except that in the present study the two oppositely directed beams were steered collinearly through the fluorescence cell rather than at a small angle. Feedback to the dye laser was eliminated by placing a polarizer in the incoming beam and a polarization rotator after the beam splitter in the region where the beams are separated. The proper set-

[a)]This work supported by National Science Foundation Grant No. CHE76-06103 and Grant No. C-586 from the Robert A. Welch Foundation.
[b)]National Research Council of Canada Postdoctoral Fellow 1976–78.
[c)]Permanent address: Institut für Atom und Festkörperphysik, Freie Universität Berlin, Berlin, Germany.

 0021-9606/79/010042-08$01.00

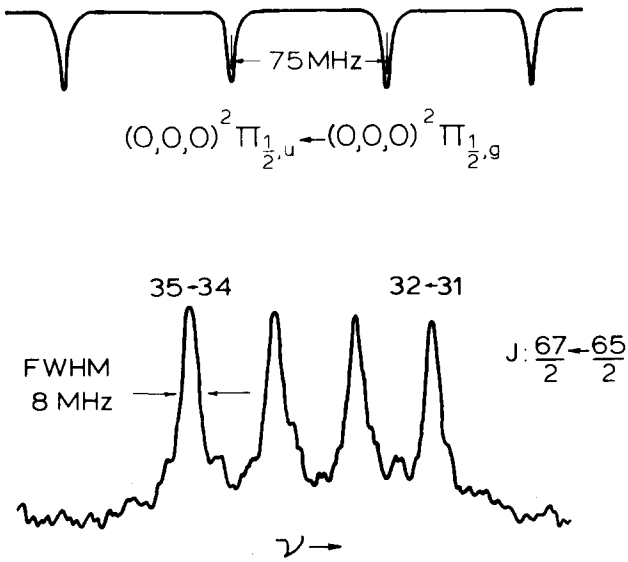

FIG. 1. Magnetic hyperfine structure of $(0,0,0)\ ^2\Pi_{1/2,u} \leftarrow (0,0,0)\ ^2\Pi_{1/2,g}$, J: $\frac{67}{2} \leftarrow \frac{65}{2}$ due to the ^{11}B nuclear spin as observed with intermodulated fluorescence saturation spectroscopy.

ting of the rotator was then found so that all returning beams were absorbed by the polarizer. Frequency markers were generated by monitoring the transmission of a one meter confocal cavity through which a portion of the laser output was directed. The markers, spaced at 75 MHz intervals, were detected with a photodiode and the resulting voltage applied to one of the Y channels of an XYY recorder. The output of the PMT was phase sensitive detected and fed to the other Y channel while the X channel was driven by the scan voltage that was simultaneously being applied to the dye laser output mirror and air-spaced etalon.

OBSERVATIONS

Saturation spectra were obtained for 22 lines of the $\tilde{A}\,^2\Pi_u(0,0,0) \leftarrow \tilde{X}\,^2\Pi_g(0,0,0)$ electronic band of $^{11}BO_2$: 10 transitions from the $^2\Pi_{3/2,u} \leftarrow {}^2\Pi_{3/2,g}$ subband (bandhead at 18320.6 cm^{-1}) and 12 transitions from the $^2\Pi_{1/2,u} \leftarrow {}^2\Pi_{1/2,g}$ subband (bandhead at 18273.5 cm^{-1}). In addition, 15 lines from the $^2\Sigma_g^+(0,1,0) \leftarrow {}^2\Sigma_u^+(0,1,0)$ vibronic subband (bandheads at 18390.8 cm^{-1} and 18385.6 cm^{-1}) were detected. Only R-type transitions were used in the present analysis since none of the P-type lines observed (all high J) had resolvable hyperfine splittings. The hyperfine structure detected in this study can be attributed to the interaction of the ^{11}B nuclear magnetic moment with the magnetic fields due to the electron spin and the electron orbital motion. It is not expected that splittings due to interaction of the nuclear electric quadrupole moment with the electric field gradient at the nucleus make an important contribution to the overall splitting pattern. An example of the hyperfine structure, showing the four components of the transitions, is given in Fig. 1.

The typical linewidth (FWHM) for a single hyperfine component was 8 MHz. Since the medium term stability of the dye laser was found to be ±1 MHz, the dominant contributions to this linewidth are likely natural lifetime broadening and power broadening.[10] From the recent measurements of the radiative lifetimes of the $^2\Pi_u(0,0,0)$ and $^2\Sigma_g^+(0,1,0)$ excited states of BO_2,[11] the natural linewidth is of the order of 4 MHz. Power broadening was particularly noticeable during the early stages of the experiment when 20 mW of dye laser power was focused to a 100 μ beam waist. Under these conditions, test spectra of NH_2 were produced with linewidths of 6 MHz, but, as shown in Fig. 2a, the hyperfine components of a BO_2 transition were seriously broadened. The poor resolution obtained in the earlier saturation work on BO_2[2] may be due, at least in part, to such broadening. Reduction of the dye laser output power by a factor of fifty resulted in considerable improvement in the linewidth, as shown in Fig. 2b. Further reduction of the power gave a lower signal-to-noise ratio without a significant narrowing (see Fig. 2c). Rather than attenuate the laser power to such a large extent, we chose to defocus the beams entering the fluorescence cell to lower intensities and achieve the same linewidth.

The overall hyperfine splittings from the highest frequency to the lowest frequency component ranged in value from 130 MHz to less than 20 MHz. The three series studied exhibited different dependencies on the total angular momentum quantum number J. From Fig. 3c, it can be seen that the splittings of the $^2\Pi_{3/2,u} \leftarrow {}^2\Pi_{3/2,g}$ transitions initially decrease with an increase in J. For higher J values, however, the splittings become J independent with an average value of 20 MHz. That this asymptotic value does not more closely approach zero is a clear indication of the breakdown of pure Hund's case (a) coupling for larger values of J through a mixing of $^2\Pi_{3/2}$ with the $^2\Pi_{1/2}$ state. The splitting trends for

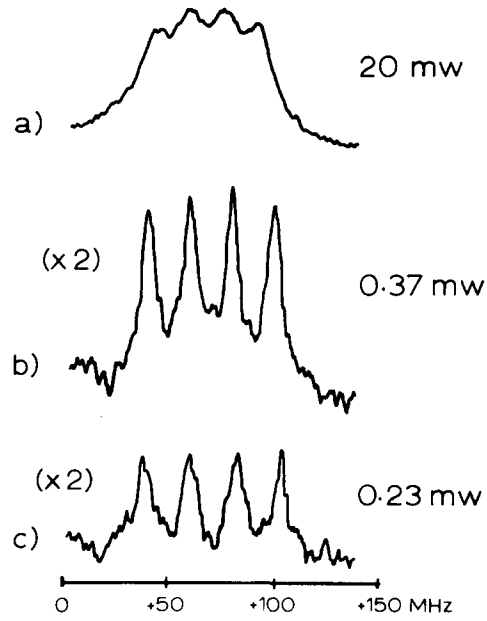

FIG. 2. The effects of power broadening on the hyperfine linewidths of BO_2. (a) At 20 mW the hyperfine structure is barely resolved. (b) Reduction in the laser power by a factor of fifty to 0.37 mW has resulted in a marked improvement in linewidth. (c) Further reduction of laser power yields no significant improvement in resolution.

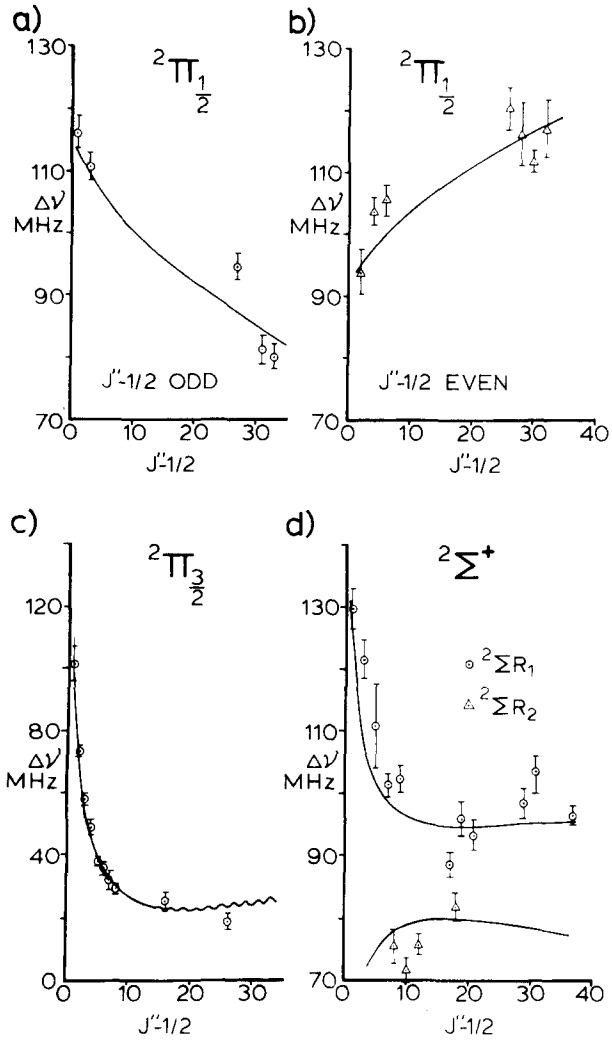

FIG. 3. Examples of the strong J dependence of the overall hyperfine splitting frequency, where $\Delta\nu$ is measured from a zero point corresponding to the lowest F component of a given line. The splitting trends are seen to be characteristic of the subband to which the transitions belong. For Figs. 3b and 3d the splittings of the lines marked with a △ are, in fact, the negative of the value shown since their highest F component lies to lower frequency than the lowest F component. The solid curves were determined from the constants given in Table III. The oscillations at higher J in the calculated value in Fig. 3c arise from d' as a result of mixing in of $^2\Pi_{1/2}$. Finally, the error bars correspond to an estimated $\pm 2\sigma$ of the observed splittings.

the $^2\Pi_{1/2,u} \leftrightarrow {}^2\Pi_{1/2,g}$ transitions are less straightforward. This is due both to mixing of $^2\Pi_{1/2}$ with $^2\Pi_{3/2}$ and to the presence of the hyperfine doubling constant, d,[12] which affects, to first order, the energy levels of the Ω doublets in $^2\Pi_{1/2}$ states alone, giving equal and opposite contributions to each member of the Ω doublet. In the case of BO_2, which belongs to the point group $D_{\infty h}$, the levels antisymmetric with respect to interchanging the two oxygen nuclei are missing since the equivalent nuclei obey Bose statistics and have zero nuclear spin. As a result, only one of the Ω doublet components is present for a given J [13] and the sign of the d contribution to the hyperfine splittings depends on the evenness or oddness of $J'' - \frac{1}{2}$. This is shown in Fig. 3b. It is interesting to note that the hyperfine labelling of the transitions for which $J'' - \frac{1}{2}$ is odd proceeds toward higher frequency with increasing F value just as for the lines in $^2\Pi_{3/2,u} \leftrightarrow {}^2\Pi_{3/2,g}$. For $J'' - \frac{1}{2}$ even, the highest $F'' + 1 \leftrightarrow F''$ component appears at the lowest frequency. This labeling alteration results because the hyperfine splittings in the $^2\Pi_{1/2}$ spectrum are dominated by d'.

The splittings of the $^2\Sigma_g^+(0, 1, 0)$ transitions can also be divided into two categories according to whether the line originates from the upper (R_1) or the lower (R_2) spin rotation doublet level of the $^2\Sigma_u^+$ state (see Fig. 3d). For these hotband transitions, the F labeling increases with increase in frequency for the R_1 lines and decreases for the R_2 lines.

Associated with the problems of unravelling the J dependence of the hyperfine splittings, a further complicating feature arose in the assignment of the transitions. It was not uncommon for a high J and a low J transition to fall within the same Doppler profile, a fact which would lead to assignment ambiguities unless some means could be found to differentiate between the lines belonging to each transition. Fortunately, transitions with widely disparate J values could be distinguished on the basis of the intensity distribution pattern of the hyperfine components. Moreover, the low J transitions ($J'' - \frac{1}{2} < 5$) were characterized by the presence of crossover signals[14] which are not observed for the high J lines because $\Delta F \neq \Delta J$ transitions become progressively weaker with increasing J. Finally, it should be noted that interference from $^{10}BO_2$ transitions was not a problem since with a spin of 3 for the ^{10}B nucleus, a typical R-branch transition would be split into seven hyperfine components rather than the four due to ^{11}B.

Although the short (>100 μsec) and medium (up to 15 sec) term stability of the dye laser and reference cavity are better than 1 MHz, the long term stability (~300 sec) of neither is better than 10–20 MHz. We have recently found that slight variations in the atmospheric pressure in the laboratory are the principal cause of this long term frequency drift. (A 5 mtorr change in pressure corresponds to a frequency shift of about 1 MHz.) For the measurements described here the somewhat paradoxical situation exists that it is not possible to measure accurately the hyperfine spacings because of poor reproducibility and linearity of the frequency scale even though the resolution is very high.

Each of the 37 transitions studied was scanned and measured at least twice. The quality of a scan was judged primarily on the uniformity of the reference cavity marker spacings and was given a weighting in determining the hyperfine spacings of that transition inversely proportional to the square of estimated uncertainty in the spacings. This uncertainty arises both from the non-uniformity in the markers and the error in measuring the peak positions and both effects were included in its estimation. These weights were also used in the least squares analysis to be described later. The measured hyperfine splittings are given in Table I.

TABLE I. Observed[a] and calculated hyperfine splittings (MHz).

$^2\Pi_{3/2,u}(0,0,0) \leftarrow {}^2\Pi_{3/2,g}(0,0,0)$[b]				$^2\Pi_{1/2,u}(0,0,0) \leftarrow {}^2\Pi_{1/2,g}(0,0,0)$[b]			
J''	$F' \leftarrow F''$	$\Delta\nu$ Obs	$\Delta\nu$ Calc	J''	$F' \leftarrow F''$	$\Delta\nu$ Obs	$\Delta\nu$ Calc
1.5	1←0		•••	1.5	1←0		•••
	2←1	16.9	19.8		2←1	29.1	27.1
	3←2	52.0	56.8		3←2	69.6	65.2
	4←3	101.5	110.7		4←3	116.2	114.4
2.5	2←1		•••	2.5	2←1	93.9	95.6
	3←2	17.3	17.1		3←2	72.3	72.2
	4←3	39.7	41.9		4←3	41.5	40.4
	5←4	73.4	74.5		5←4		•••
3.5	3←2		•••	3.5	3←2		•••
	4←3	14.7	14.6		4←3	28.8	29.7
	5←4	34.2	33.6		5←4	65.6	66.5
	6←5	57.8	57.3		6←5	110.8	110.5
4.5	4←3		•••	4.5	4←3	103.7	97.9
	5←4	12.2	12.7		5←4	76.4	70.9
	6←5	29.9	28.4		6←5	42.0	38.2
	7←6	49.0	47.0		7←6		•••
5.5	5←4		•••	6.5	6←5	105.5	100.3
	6←5	10.3	11.3		7←6	76.0	71.1
	7←6	23.7	24.8		8←7	40.9	37.7
	8←7	37.8	40.5		9←8		•••
6.5	6←5		•••	26.5	26←25	120.3	114.8
	7←6	10.0	10.3		27←26	82.5	77.9
	8←7	24.6	22.2		28←27	41.4	39.6
	9←8	35.4	35.8		29←28		•••
7.5	7←6		•••	27.5	27←26		•••
	8←7	9.2	9.5		28←27	31.9	28.4
	9←8	19.7	20.4		29←28	63.5	57.8
	10←9	31.7	32.6		30←29	94.7	88.2
8.5	8←7		•••	28.5	28←27	116.2	115.9
	9←8	8.3	8.9		29←28	80.0	78.6
	10←9	17.7	18.9		30←29	41.3	39.9
	11←10	29.0	29.9		31←30		•••
16.5	16←15		•••	30.5	30←29	111.7	117.0
	17←16	7.1	7.1		31←30	76.4	79.2
	18←17	15.0	14.6		32←31	39.2	40.2
	19←18	25.1	22.6		33←32		•••
26.5	26←25		•••	31.5	31←30		•••
	27←26	5.3	7.3		32←31	27.4	27.7
	28←27	10.2	14.9		33←32	55.1	56.2
	29←28	18.6	22.8		34←33	81.3	85.6
				32.5	32←31	117.1	118.1
					33←32	80.1	79.9
					34←33	40.8	40.5
					35←34		•••
				33.5	33←32		•••
					34←33	26.9	27.3
					35←34	53.1	55.4
					36←35	80.1	84.3

$^2\Sigma_g^+(0,1,0) \leftarrow {}^2\Sigma_u^+(0,1,0)$[b]				$^2\Sigma_g^+(0,1,0) \leftarrow {}^2\Sigma_u^+(0,1,0)$[b]			
R_1 Branch				R_2 Branch			
J''	$F' \leftarrow F''$	$\Delta\nu$ Obs	$\Delta\nu$ Calc	J''	$F' \leftarrow F''$	$\Delta\nu$ Obs	$\Delta\nu$ Calc
1.5	1←0		•••	8.5	8←7	75.4	77.5
	2←1	22.8	22.2		9←8	53.2	54.5
	3←2	66.2	65.3		10←9	27.3	28.7
	4←3	129.7	129.4		11←10		•••

TABLE I (*Continued*)

	$^2\Sigma_g^+(0,1,0) \leftarrow {}^2\Sigma_u^+(0,1,0)$[b]				$^2\Sigma_g^+(0,1,0) \leftarrow {}^2\Sigma_u^+(0,1,0)$[b]		
	R_1 Branch				R_2 Branch		
J''	$F' \leftarrow F''$	$\Delta\nu$ Obs	$\Delta\nu$ Calc	J''	$F' \leftarrow F''$	$\Delta\nu$ Obs	$\Delta\nu$ Calc
3.5	3←2		•••	10.5	10←9	71.6	78.4
	4←3	32.0	27.0		11←10	54.1	54.7
	5←4	72.5	62.8		12←11	28.0	28.5
	6←5	121.6	107.5		13←12		•••
5.5	5←4		•••	12.5	12←11	75.8	79.0
	6←5	31.7	28.2		13←12	53.1	54.7
	7←6	69.3	61.9		14←13	27.2	28.4
	8←7	110.9	101.2		15←14		•••
7.5	7←6		•••	18.5	18←17	81.7	79.4
	8←7	29.8	28.7		19←18	56.5	54.4
	9←8	63.6	61.5		20←19	30.4	27.9
	10←9	101.3	98.4		21←20		•••
9.5	9←8		•••				
	10←9	30.7	29.1				
	11←10	65.5	61.3				
	12←11	102.4	96.8				
17.5	17←16		•••				
	18←17	28.7	29.9				
	19←18	57.9	61.5				
	20←19	88.5	94.9				
19.5	19←18		•••				
	20←19	30.9	30.0				
	21←20	63.3	61.6				
	22←21	95.9	94.8				
21.5	21←20		•••				
	22←21	31.0	30.2				
	23←22	61.6	61.8				
	24←23	93.3	94.8				
29.5	29←28		•••				
	30←29	32.8	30.7				
	31←30	65.5	62.4				
	32←31	98.5	95.2				
31.5	31←30		•••				
	32←31	34.2	30.8				
	33←32	68.7	62.6				
	34←33	103.6	95.4				
37.5	37←36		•••				
	38←37	32.7	31.1				
	39←38	64.3	63.1				
	40←39	96.5	95.9				

[a]The splittings have been measured from the lowest frequency $F+1 \leftarrow F$ transition to each successive transition.

[b]R branch transitions only. $J' = J'' + 1$.

ANALYSIS

The magnetic hyperfine parameters which determine the hyperfine structure of BO_2 may be expressed as[12]:

$$a = \frac{2\mu_0\mu_I}{I}\left\langle\frac{1}{r^3}\right\rangle_{av} \tag{1a}$$

$$b = \frac{2\mu_0\mu_I}{I}\left[\tfrac{8}{3}\pi\psi^2(0) - \left\langle\frac{3\cos^2\theta - 1}{2r^3}\right\rangle_{av}\right] \tag{1b}$$

$$c = \frac{3\mu_0\mu_I}{I}\left\langle\frac{3\cos^2\theta - 1}{r^3}\right\rangle_{av} \tag{1c}$$

$$d = \frac{3\mu_0\mu_I}{I}\left\langle\frac{\sin^2\theta}{r^3}\right\rangle_{av}, \tag{1d}$$

where μ_0 is the Bohr magneton, μ_I is the nuclear magnetic moment and I is the nuclear spin. A total of eight hyperfine constants are, therefore, required for the characterization of the hyperfine splittings, four for the $\tilde{X}\ ^2\Pi_g$ ground state and four for the $\tilde{A}\ ^2\Pi_u$ excited state. These constants are related to those of Muirhead *et al.*,[2] in the following manner:

TABLE II. Hamiltonian matrix for the $^2\Pi$ electronic states including hyperfine structure.

	$\Omega=\pm\frac{3}{2}$	$\Omega=\pm\frac{1}{2}$
$\Omega=\pm\frac{3}{2}$	$\frac{1}{2}A-B+B[(J+1/2)^2-1/2]+\frac{3}{2}\frac{\mathbf{I}\cdot\mathbf{J}}{2J(J+1)}\left[a+\frac{b+c}{2}\right]$	$\left[\frac{\mathbf{I}\cdot\mathbf{J}}{4J(J+1)}b-B\right][(J+1/2)^2-1]^{1/2}$
$\Omega=\pm\frac{1}{2}$	$\left[\frac{\mathbf{I}\cdot\mathbf{J}}{4J(J+1)}b-B\right][(J+1/2)^2-1]^{1/2}$	$-\frac{1}{2}A+B+B[(J+1/2)^2-1/2]+\frac{1}{2}\frac{\mathbf{I}\cdot\mathbf{J}}{2J(J+1)}\left[a-\frac{b+c}{2}+2(-1)^{J-1/2+p}(J+1/2)d\right]$[a]

[a]In the diagonal element for $^2\Pi_{1/2}$, p is 0 for the $\tilde{A}\,^2\Pi_u$ state and is 1 for the $\tilde{X}\,^2\Pi_g$ state.

This work	Ref. 2
a	a
$b+c/3$	b
c	$3c$

d is not involved in the $^2\Sigma_g^+(0,1,0)-{}^2\Sigma_u^+(0,1,0)$ hyperfine structure studied by Muirhead, *et al.*,[2] and is, therefore, not listed above. The interpretation of a, b, c, and d in terms of electronic nuclear magnetic interactions is discussed by Frosch and Foley.[12]

For the $^2\Sigma_g^+-{}^2\Sigma_u^+$ transitions, the Hamiltonian used was that of Muirhead, *et al.*,[2] with the appropriate changes to correct for differences in definition of the constants. For the $^2\Pi_u-{}^2\Pi_g$ transitions, the Hamiltonian given by Mizushima[15] with the centrifugal distortion terms omitted was used. The Hamiltonian matrix elements are shown in Table II. The rotational constants and Renner parameter used in this analysis for both the $\tilde{X}\,^2\Pi_g(0,0,0)$ and the $\tilde{A}\,^2\Pi_u(0,0,0)$ electronic states were those of Johns.[8] Also, in including transitions from the $^2\Sigma_g^+(0,1,0)-{}^2\Sigma_u^+(0,1,0)$ subband with those from the $^2\Pi_u(0,0,0)-{}^2\Pi_g(0,0,0)$ manifold, we have ignored any vibrational dependence of A, B, or the hyperfine constants.[16]

Once the appropriate Hamiltonian matrices were chosen by the process just described, the eigenvalues were obtained by matrix diagonalization. Note that this approach gives results which do not depend on a coupling scheme.

From the energy levels thus computed, transition frequencies may be calculated. These frequencies are given by a linear combination of hyperfine coupling constants plus a center frequency for the optical transition. By using for this center frequency the average of the four completely allowed hyperfine components instead of a hypothetical frequency in the absence of hyperfine structure, it is possible to separate the fitting of the line center (just the average of the frequencies of the four components) from the determination of the hyperfine coupling constants and arrive at a computational problem which is simply a least squares fit of the displacement of the hyperfine components from the average value with eight hyperfine coupling constants.

Our intent was to fit the 37 observed transitions appropriately weighted to reflect the data quality with eight hyperfine coupling parameters. However, in order to determine how many of these hyperfine coupling constants are determined, we diagonalized the matrix of coefficients of the normal equations and examined the magnitudes of the eigenvalues. Well determined linear combinations of the parameters are those eigenvectors associated with large positive eigenvalues. Unfortunately, only three of the eigenvalues were judged large enough for the corresponding linear combinations to be adequately determined with a fourth marginally determined. One can fit on the well determined parameters[17] only and this was done. It was found that the inclusion of the fourth linear combination resulted in a substantial improvement in the standard deviation of the fit, indicating that this linear combination is larger than anticipated.

At this stage of the analysis, in lieu of sufficient information to evaluate the eight constants, we chose to supplement the existing data by including as additional observations (with variable weights) the following assumptions based upon a plausible electronic structure for BO_2.

(i) $3a'-c'-3d'=0$ (2)

Equation 2 followed directly from the defining equations of a, c, and d.[12]

(ii) $a''=0$ (3a)

$c''=0$ (3b)

$d''=0$ (3c)

If one restricts the basis functions to include only s and p orbitals, the probability that the lone pair electron in the $^2\Pi_g$ state resides on the boron atom is zero. Since a'', c'', and d'' are all proportional to $\langle 1/r^3\rangle_{av}$, where r is the distance from the nucleus to the electron, their values under this assumption are approximately equal to zero. Of course, b'' would also be predicted to be zero, but it is well known that isotropic coupling constants are not negligible in situations such as this as the result of spin polarization.[18]

(iii) $a'-\frac{5}{6}d'=0$ (4)

This is a consequence of the assumption that the lone electron in the $^2\Pi_u$ state is localized in a purely p orbital perpendicular to the figure axis.

The choice made here of introducing assumptions as data in order to condition the least squares rather than employing the diagnostic least squares procedure[17] was dictated by the nature of the assumptions we wished to make. In diagnostic least squares one has an *a priori* guess for

TABLE III. Calculated hyperfine constants (in MHz).

$\tilde{A}\,^2\Pi_u$	$\tilde{X}\,^2\Pi_g$
$a' = 45.9$	$a'' = 0.5$
$b' = 9.4$	$b'' = -71.8$
$c' = -68.8$	$c'' = 0.1$
$d' = 68.2$	$d'' = -0.2$

each parameter with a guessed uncertainty. Assumption (ii) can easily be cast in that form, but assumptions (i) and (iii) describe a *relationship* expected to hold and are not in the usual form appropriate to diagnostic least squares. These assumptions can be used in the diagnostic least squares method by using a nondiagonal *a priori* covariance matrix as was discussed in the Appendix of Ref. 17.

Using this method and giving (i) a weight of 0.5, (ii) a weight of 10, and (iii) a weight of 0.5, we were able to make estimates shown in Table III of the eight magnetic hyperfine coupling constants which fit the observations and are physically reasonable. Of course, these estimates are only one set of many possible solutions which are consistent with the observations, and have been chosen for their "reasonableness."

DISCUSSION

Since the constants are determined partly by assumption, we feel that a detailed discussion of their interpretation in terms of the electronic structure is not warranted. However, it is important to understand why a unique set of coupling constants was not obtained from the present data and what kind of data could lead to substantially improved determination. Part of the problem undoubtedly lies with the precision of the measurements. Despite a significant improvement in spectral resolution over previous efforts[2,19] allowing the spacings between adjacent hyperfine components to be easily measured, drifts in both the marker cavity and the reference cavity combined with nonlinearities in the response of the end mirror PZT on the reference cavity led to uncertainties in the frequency scale. As mentioned above, it appears that the cavity drifts are associated primarily with atmospheric pressure changes and that substantial improvement is obtained upon evacuation of the cavities. These problems of frequency drift and scale nonlinearities can be overcome almost completely by introducing a second feedback loop into the stabilization scheme. As shown by Gerhardt and Timmermann,[7] the output of the reference cavity can be compared against a Lamb-dip or iodine stabilized He–Ne laser and the resulting error signal applied to the reference cavity PZT. In this way, frequency calibration to ±100 KHz can be achieved. Unfortunately, this second feedback loop system has the disadvantage of being quite expensive to construct.

Even with very accurate frequency calibration of the data, the problem of the indeterminacy of the constants would remain. The indeterminacies found here largely arise because the splittings between adjacent F components are not explicitly dependent upon the hyperfine constants of either the upper or lower electronic state of the transition but upon their difference, with the result that it is very difficult to extract information about one state that is independent of the other state. This observation is not new, of course. Spectroscopists concerned with the analysis of vibration-rotation structure under Doppler-limited conditions have long been aware that the difference $B' - B''$ is quite sensitive to the input data while the values of B' and B'' themselves are not. In the case of rotational constants, this difficulty can be reduced to a considerable extent by measuring transitions from as many subbranches as possible, permitting the use of combination differences to obtain information which depends on one state or the other but not both. Unfortunately, this approach is not particularly applicable to the hyperfine structure of BO_2. The few P branch lines that could be observed in the present study were generally high J transitions whose hyperfine structure was not resolvable with our instrument.

Given the above limitations of the present data, the best approach appears to be to find an experimental technique which can probe the hyperfine structure of each electronic state. Recently,[20] microwave optical double resonance (MODR) has been successfully employed to probe the ground and excited states of NH_2. However, BO_2 is not a very suitable molecule for MODR study in that the transitions in the accessible microwave region (2–18 GHz) are limited to the magnetic dipole transitions between the low N, spin rotation doublet levels in the $^2\Sigma_u^+(0,1,0)$ and $^2\Sigma_g^+(0,1,0)$ vibronic states. The experiment would nonetheless provide needed additional information and should be attempted.

Note added in proof. Recently Kim, Smalley, and Levy [J. Mol. Spectrosc. 71, 458 (1978)] reported observations in a magnetic field of MODR on the 5145 Å coincidence in BO_2.

[1]D. K. Russell, M. Kroll, R. A. Beaudet, and D. A. Dows, Chem. Phys. Lett. **20**, 153 (1973); D. K. Russell, M. Kroll, and R. A. Beaudet, J. Chem. Phys. **66**, 1999 (1977).
[2]A. Muirhead, K. V. L. N. Sastry, R. F. Curl, Jr., J. Cook, and F. K. Tittel, Chem. Phys. Lett. **24**, 208 (1974).
[3]A. Fried and C. W. Mathews, Chem. Phys. Lett. **52**, 363 (1977).
[4]R. N. Dixon, D. Field, and M. Nobel, Chem. Phys. Lett. 50, 1 (1977).
[5]R. A. Beaudet, Seventh Austin Symposium on Gas Phase Molecular Structure, March 1978, Paper TM2.
[6]R. L. Barger, M. S. Sorem, and J. L. Hall, Appl. Phys. Lett. **22**, 573 (1973).
[7]H. Gerhardt and F. K. Tittel, Opt. Commun. **16**, 307 (1976); H. Gerhardt and A. Timmermann, *ibid.* **21**, 343 (1977).
[8]J. W. C. Johns, Can. J. Phys. **39**, 1738 (1961).
[9]M. S. Sorem and A. L. Schawlow, Opt. Commun. **5**, 148 (1972).
[10]V. S. Letokhov and V. P. Chebotayev, *Nonlinear Laser Spectroscopy* (Springer-Verlag, Berlin, 1977), pp. 12–17.
[11]B. A. Thrush, Chem. Phys. Lett. **55**, 404 (1978).
[12]R. A. Frosch and H. M. Foley, Phys. Rev. **88**, 1337 (1952).
[13]G. Herzberg, *Molecular Spectra and Molecular Structure*, 2nd ed. (Van Nostrand Reinhold, New York, 1950), Vol. 1, p. 268.

[14]H. Schlossberg and A. Javan, Phys. Rev. **150,** 267 (1966).
[15]M. Mizushima, *The Theory of Rotating Diatomic Molecules* (Wiley, New York, 1975), p. 278.
[16]D. K. Russell and R. A. Beaudet, Mol. Phys. **27,** 1645 (1974).
[17]R. F. Curl, J. Comp. Phys. **6,** 367 (1970).
[18]M. Karplus and G. Fraenkel, J. Chem. Phys. **35,** 1312 (1961).
[19]G. W. Hills, D. L. Philen, R. F. Curl, Jr., and F. K. Tittel, Chem. Phys. **12,** 107 (1976).
[20]J. M. Cook, G. W. Hills, and R. F. Curl, Jr., J. Chem. Phys. **67,** 1450 (1977), and references therein.